Structural and thermal stability criteria of Bi_2O_3–B_2O_3 glasses

2008 J. Phys.: Condens. Matter 20 155108

(http://iopscience.iop.org/0953-8984/20/15/155108)

J. Phys.: Condens. Matter **20** (2008) 155108 (9pp) doi:10.1088/0953-8984/20/15/155108

Structural and thermal stability criteria of Bi_2O_3–B_2O_3 glasses

Essam R Shaaban[1], M Shapaan[2] and Yasser B Saddeek[1,3]

[1] Physics Department, Faculty of Science, Al-Azhar University, PO 71452, Assiut, Egypt
[2] Physics Department, Faculty of Science, Al-Azhar University, Cairo, Nasr City, Egypt

E-mail: esam_ramadan2005@yahoo.com

Received 18 December 2007, in final form 16 February 2008
Published 25 March 2008
Online at stacks.iop.org/JPhysCM/20/155108

Abstract

Glasses with compositions $x Bi_2O_3$–$(100 - x)B_2O_3$ with $30 \leqslant x \leqslant 60$ mol% have been prepared using the normal melt quenching technique. Infrared (IR) spectroscopy was used as a structural probe of the nearest-neighbor environment in the glass network. Assessment of the thermal stability of these glasses was achieved in terms of various simple quantitative methods based on the characteristic temperatures, such as the glass transition temperature, T_g, the onset temperature of crystallization, T_{in}, the temperature corresponding to the maximum crystallization rate, T_p, and the melting temperature, T_m. In this case, k_{gl} may be more suitable for estimating the glass thermal stability in the above composition range. In this work the kinetic parameter $K_r(T)$ is added to the stability criteria. The thermal stability of the glasses that were studied has been correlated with the activation energy of crystallization by this kinetic criterion and compared with those evaluated by other criteria. The results of both the criteria and the kinetic parameter $K_r(T)$ confirm that the thermal stability decreases with increasing Bi_2O_3 content. The former parameters, besides the average force constant of the BO_3 structural unit, were characterized and discussed in terms of the changes in the glass structure.

(Some figures in this article are in colour only in the electronic version)

1. Introduction

B_2O_3 is one of the most important glass formers incorporated into various kinds of glass systems as a flux material in order to attain materials with specific physical and chemical properties suitable for high-technological applications. The boron atom in borate crystals and glasses usually coordinates with either three or four oxygen atoms, forming $[BO_3]$ or $[BO_4]$ structural units. These two fundamental units can be combined arbitrarily to form either the so-called super structure or different B_xO_y structural groups like boroxol ring, pentaborate, tetraborate, diborate groups etc. The number of structural units depends on the nature and the total concentration of the added modifiers [1–5].

In terms of the crystalline configuration, Bi_2O_3 is a higher valency oxide and has low field strength and high polarizability, so its glassy phase cannot be obtained, in contrast to pure B_2O_3 glass. However, in the presence of very small additions of conventional glass formers (e.g. B_2O_3), it may build a glass network of $[BiO_3]$ pyramids [6, 7]. Also, it was suggested that Bi_2O_3 can occupy both network forming and network modifying positions in the borate glasses and, as a result, the physical properties of such glasses exhibit discontinuous changes when the structural role of the cation was switching over in this way [8–10].

On these bases, glasses containing Bi_2O_3 have attracted considerable attention due to their wide applications in the field of glass-ceramics, thermal and mechanical sensors, reflecting windows, or their use as layers for optical and opto-electronic devices, etc [11–19]. These glasses have a long infrared cut-off, and high third-order nonlinear optical susceptibility, which makes them ideal candidates for applications as infrared transmission components, ultrafast optical switches, and photonic devices [20, 21]. Recent studies by infrared (IR), ultraviolet–visible (UV–vis) and thermal analysis on bismuthate-based glasses revealed the presence of distorted BiO_6 polyhedra as the main structural unit in these glasses [22–24].

In view of the aforementioned perspective, the aim of the present work is to investigate the influence of Bi_2O_3 on the

[3] Author to whom any correspondence should be addressed.

structure and the thermal stability of the borate glasses by means of IR and differential thermal analysis (DTA).

2. Experimental procedures

2.1. Glass preparation

The glass samples having the general chemical formula $x\mathrm{Bi_2O_3}$–$(100-x)\mathrm{B_2O_3}$ with $30 \leqslant x \leqslant 60$ mol% have been prepared by the melt quenching technique. Required quantities of Analar grade $\mathrm{Bi_2O_3}$, and $\mathrm{H_3BO_3}$ were mixed together by grinding the mixture repeatedly to obtain a fine powder. The mixture was melted in a porcelain crucible in an electrically heated furnace under ordinary atmospheric conditions at a temperature of about 1273 K for 2 h to homogenize the melt. The glass samples obtained from quick melt quenching into a pre-heated stainless steel mold were heat-treated at a temperature of about 20 K below their calorimetric glass transition temperature for 2 h to remove any internal stresses. The composition refers to the nominal composition (the starting mixture).

2.2. Glass characterization

In order to check the non-crystallinity of the glass samples, x-ray diffraction (XRD) measurements were performed using a Philips x-ray diffractometer PW/1710 with Ni-filtered, Cu Kα radiation ($\lambda = 1.542$ Å) powered at 40 kV and 30 mA. The results showed that XRD patterns of the glasses (not shown) did not reveal any discrete or sharp peaks, but the characteristic broad humps of the amorphous materials.

Infrared absorption spectra of the glasses in the wavenumber range 400–2000 $\mathrm{cm^{-1}}$ with a resolution of 4 $\mathrm{cm^{-1}}$ were recorded at room temperature using an infrared spectrophotometer type JASCO, FT/IR—430 (Japan), using the KBr pellet technique. The infrared spectra were corrected for the dark-current noises, and normalized to eliminate the concentration effects of the powder sample in the KBr disc. The resulting spectra are deconvoluted to enable us to shed further light on the structural changes of $\mathrm{BO_3}$ triangles and $\mathrm{BO_4}$ tetrahedra, as they are the most abundant units in these glasses. The change in the stretching force constant, $F_{\mathrm{M-O}}$, of B–O, and Bi–O bonds in these glasses was obtained by applying an equation reported by Shelby [1] as,

$$F_{\mathrm{M-O}} = 4\pi^2 c^2 \mu \nu_{\mathrm{eff}}^2 \tag{1}$$

where c is the speed of light, μ is the reduced mass of the cation site, and ν_{eff} is the effective cation site vibration frequency. The corresponding bond length, r (nm), can be given by an empirical formula suggested by Bridge *et al* [25];

$$F_{\mathrm{M-O}} = 5.28N\left[\frac{X_a X_b}{r^2}\right]^{3/4} + 30\ (\mathrm{N\,m^{-1}}) \tag{2}$$

where N is the bond order (1, 2, or 3), and X_a and X_b are the electronegativities of the anion and the cation, respectively.

Calorimetric measurements were carried out by differential thermal analysis using a Shimadzu 50 with an accuracy of ±0.1 K. The calorimeter was calibrated, for each heating rate, using the well-known melting temperatures and melting enthalpies of zinc and indium supplied with the instrument. Powdered samples of 20 mg were crimped into aluminum pans and scanned at continuous heating rates ($\beta = 5$, 10, 20, 30, 40 K $\mathrm{min^{-1}}$). The values of the glass transition temperature, T_{g}, the extrapolated crystallization onset temperature, T_{in} and the crystallization peak temperature, T_{p}, were determined with accuracy of ±1 K by using the microprocessor of the thermal analyzer.

3. The criterion parameters of thermal stability

The criterion parameters are based on characteristic temperatures such as the glass transition temperature, T_{g}, the onset temperature of crystallization T_{in}, the crystallization temperature, T_{p}, and the melting temperature, T_{m}. Dietzel [26] introduced the glass criterion, $\Delta T = T_{\mathrm{in}} - T_{\mathrm{g}}$, which is often an important parameter for evaluating the glass forming ability. The thermal stability of glasses according to Sakka and Mackenzie [27] was achieved by using the ratio $T_{\mathrm{g}}/T_{\mathrm{m}}$. By using the characteristic temperatures, Hruby [28] developed the H_r criterion, $H_r = \Delta T/(T_{\mathrm{m}} - T_{\mathrm{p}})$. Saad and Poulain [29] obtained another two criteria, the weighted thermal stability H' ($H' = \Delta T/T_{\mathrm{g}}$) and the S criterion ($S = (T_{\mathrm{p}} - T_{\mathrm{in}})\Delta T/T_{\mathrm{g}}$). The glass formation factor of the materials is given by $k_{\mathrm{gl}} = (T_{\mathrm{in}} - T_{\mathrm{g}})/(T_{\mathrm{m}} - T_{\mathrm{g}})$ and is more suitable for estimating the glass thermal stability than ΔT. The higher values of the criterion parameters reflect greater thermal stability of the glass.

On the other hand, the formal theory of transformation kinetics describes the evolution of the volume fraction that is crystallized, χ, in terms of the rate of crystal growth, u, with time t,:

$$\chi = 1 - \exp\left[-g\left(\int_0^t u\,\mathrm{d}t'\right)^n\right] = 1 - \exp(-I_1^n) \tag{3}$$

where g is a geometric factor, n is an exponent depending on the mechanism of transformation, and $I_1^n = (\int_0^t u\,\mathrm{d}t')^n$. Deriving equation (3) with respect to time and taking into account the Arrhenian temperature dependence for the crystal growth rate [30], the crystallization rate is obtained as

$$\frac{\mathrm{d}\chi}{\mathrm{d}t} = n(1-\chi)I_1^{n-1}K_0\exp\left(\frac{-E_{\mathrm{c}}}{RT}\right) = nK(1-\chi)I_1^{n-1} \tag{4}$$

where E is the effective activation energy for crystal growth and K is the reaction rate constant which has an Arrhenian temperature dependence according to the relation

$$K(T) = K_0\exp(-E_{\mathrm{c}}/RT). \tag{5}$$

Surinach *et al* [31] and Hu *et al* [32] introduced two criteria:

$$K(T_{\mathrm{g}}) = K_0\exp(-E_{\mathrm{c}}/RT_{\mathrm{g}}) \tag{6a}$$

and

$$K(T_{\mathrm{p}}) = K_0\exp(-E_{\mathrm{c}}/RT_{\mathrm{p}}). \tag{6b}$$

The values of the last two parameters indicate the tendency for glass devitrification on heating, whereas the glass formation is a kinetic process.

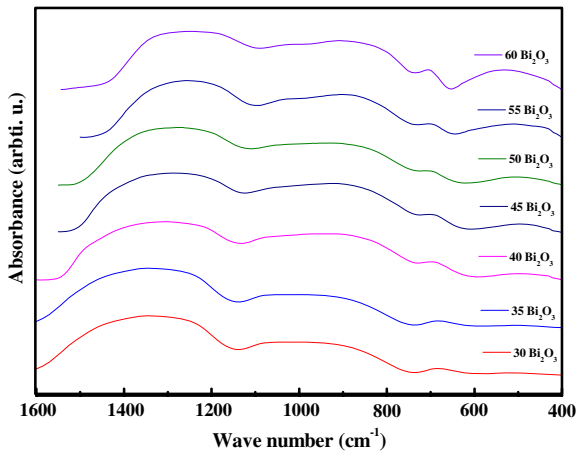

Figure 1. Infrared absorption spectra of $(100 - x)B_2O_3$–xBi_2O_3 glasses.

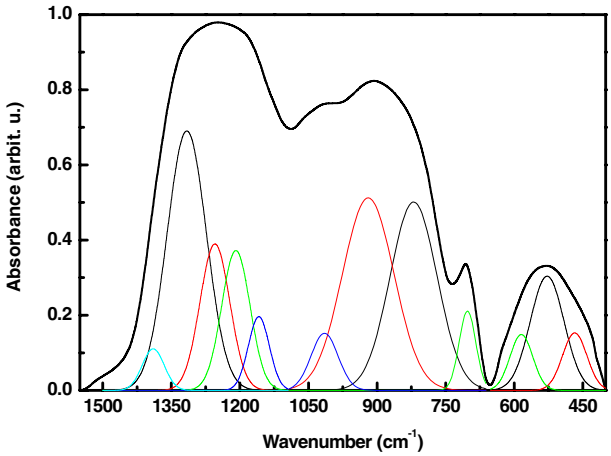

Figure 2. Band deconvolution of IR spectrum for $55B_2O_3$–$45Bi_2O_3$ glass.

The H_r parameter [33] itself is a stability factor based on characteristic temperatures, and is defined as

$$K_r(T) = K_0 \exp\left(\frac{-H_r\, E_c}{RT}\right) \tag{7}$$

where T is any temperature between T_g and T_p. The theoretical background for the definition of the parameter $K_r(T)$ was based on the analysis of the relation between the parameters $K(T)$ and $K_r(T)$. Differentiating equations (5) and (7) with respect to temperature and rewriting each parameter results in

$$\frac{\Delta K_r}{K_r \Delta T} = \frac{H_r\, E_c}{RT^2}, \qquad \frac{\Delta K}{K \Delta T} = \frac{E_c}{RT^2}. \tag{8}$$

It should be noted that the above-mentioned variation in the parameter $K_r(T)$ is H_r times the variation in parameter $K(T)$, which could justify the accuracy of the parameter. Just like the $K(T)$ criteria, the smaller the values of $K_r(T)$, the greater the thermal stability of the glass. The obvious advantage of this method is that it can evaluate the glass stability over a broad temperature range other than at only one temperature, such as T_g or T_p.

4. Results and discussion

4.1. Infrared spectral studies

In general, the IR analysis of the borate based glasses shows three distinct frequency regions: two regions, from 1100 to 1550 cm^{-1} and from 800 to 1100 cm^{-1}, which are assigned to the stretching vibrations of both triangular BO_3 and tetrahedral BO_4 borate units, respectively, and the deformation modes of both types of units are active between 600 and 800 cm^{-1} [34–36]. On the other hand, the IR analysis of Bi_2O_3 shows a frequency region extended from 400 to 600 cm^{-1}, assigned to Bi–O in BiO_6 octahedra [15, 35–38]. Thus, the incorporation of Bi_2O_3 into the borate network may cause some confusion because of the comparative wave numbers of their characteristic bands to those of some of the borate groupings. For example, the characteristic band of Bi–O may be overlapped with that attributed to the in-plane bending vibration of BO_3 units. Thus, a deconvolution process [39] should be performed to get such individual bands.

In the glasses that were studied, the systematic changes in the infrared spectra show the presence of three principal broad bands, as shown in figure 1. The observed broad bands are the result of the overlapping of individual bands with each other. Each individual band has its characteristic parameters, such as its center (C), which is related to some type of vibration of a specific structural group, and its relative area (A), which is proportional to the concentration of this structural group. Figure 2 illustrates that the deconvolution spectra of the sample contains 60 Bi_2O_3 (mol%) as an example, and the difference between the experimental and simulated curves. The spectra according to figure 1 showed some change in the center of the band around 690 cm^{-1}, while the centers of the bands around 950 and 1300 cm^{-1} were shifted to lower wavenumber, and the area of the latter bands decreases as the Bi_2O_3 content increases. Taking into consideration the expected wavenumber of Bi_2O_3 according to the length of its crystalline bonds [6, 38], one can assign the various bands listed in table 1.

The relatively intense bands at about 508–528 cm^{-1} are attributed to the vibrations of the Bi–O bonds in the BiO_6 octahedral unit. The bands ranging from 704 to 715 cm^{-1} were assigned to the bending vibrations of B–O linkages in the borate network, while the bands in the region 816–1071 cm^{-1} arise from the vibrations of the various arrangements containing BO_4 units. The bands ranging from 1209 to 1273 cm^{-1} were assigned to the stretching vibrations of the B–O bonds of $(BO_3)^{3-}$ units involving mainly the linkage oxygen connecting different groups. The band at about 1320–1361 cm^{-1} is assigned to the stretching vibrations of the B–O of trigonal $(BO_3)^{3-}$ units in metaborates, pyroborates, and orthoborates. The peaks at about 1388–1531 cm^{-1} are assigned to antisymmetrical stretching vibrations with three (NBOs) of B–O–B groups.

Before discussing the present results, it is worthwhile shedding light on the bismuth borate glasses. The characteristic vibration band of $[BiO_3]$ polyhedra at 840 cm^{-1} [8] does

Table 1. Deconvolution parameters of the infrared spectra of glasses with $30 \leqslant x \leqslant 60$. C is the component band center and A is the relative area (%) of the component band.

$x = 30$	C	—	—	—	662	704	900	975	1037	1071	1185	1222	1269	1352	1413	1466	1531
Bi_2O_3	*A*	—	—	—	0.44	0.25	7.09	8.32	2.72	1.48	0.94	5.29	11.4	28.4	4.21	16.7	5.42
$x = 35$	C	484	—	—	659	701	851	928	1013	1059	1176	1210	1255	1325	1412	1473	1516
Bi_2O_3	*A*	0.71	—	—	0.64	0.18	5.99	12.5	4.81	1.79	0.92	4.13	8.82	20.4	20.9	7.96	5.45
$x = 40$	C	452	508	—	667	710	834	896	984	1046	1175	1212	1273	1361	1433	1475	1502
Bi_2O_3	*A*	0.77	2.82	—	1.11	0.21	3.35	10.6	7.53	1.95	0.86	5.63	16	26.8	10.2	4.66	2.39
$x = 45$	C	449	489	—	675	711	831	890	971	1033	1179	1215	1268	1346	1413	1454	1483
Bi_2O_3	*A*	0.79	2.03	—	0.92	0.11	3.75	9.76	7.6	2.21	2.27	7.13	13.6	29.2	8.31	5.5	0.64
$x = 50$	C	463	514	579	663	710	839	900	978	1032	1165	1203	1250	1313	1388	1435	1472
Bi_2O_3	*A*	1.16	3.76	1	0.94	0.18	4.17	8.86	5.73	1.56	1.98	8.99	7.09	30.8	13.4	5.36	0.84
$x = 55$	C	454	497	561	670	715	816	859	922	988	1160	1199	1259	1330	1355	1389	1452
Bi_2O_3	*A*	1.52	4.27	5.02	0.58	0.15	2.23	7.88	8.72	4.01	3.48	9.07	20.5	19.3	0.09	6.7	0.04
$x = 60$	C	462	520	582	688	708	807	841	903	979	1147	1180	1241	1313	1359	1393	1422
Bi_2O_3	*A*	2.55	10.3	4.22	2.45	1.01	2.54	5.07	11.6	3.37	1.77	5.95	18	16.1	6.98	2.34	0.23

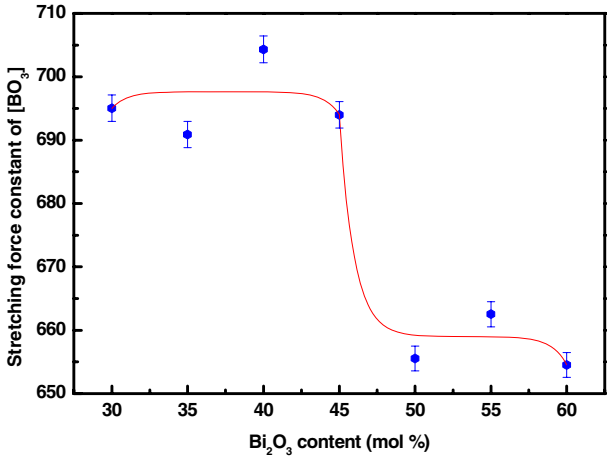

Figure 3. The compositional dependence of the stretching force constant of the $[BO_3]$ structural unit.

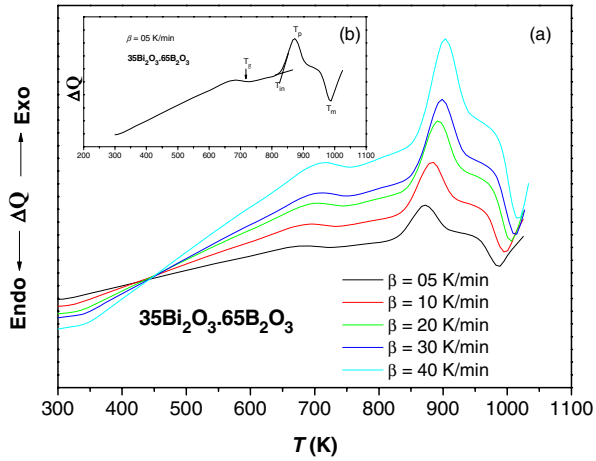

Figure 4. (a) Typical DTA trace of $35Bi_2O_3{\cdot}65B_2O_3$ glass at different heating rates. (b) Identification of T_g, T_{in}, T_p and T_m for $35Bi_2O_3{\cdot}65B_2O_3$ glass at a heating rate $\beta = 5$ K min^{-1}.

not appear in the IR spectra that are obtained, so only $[BiO_6]$ units will be expected to influence the borate network. The crystalline phase of the sample contains 30 Bi_2O_3, consisting of $3Bi_2O_3{\cdot}5B_2O_3$ which contains superstructural units in the form of isolated (i.e. not bonded to other borate units) dipentaborate groups ($B_5O_{11}^{7-}$) [4, 15]. The dipentaborate groups are formed due to the acquisition of a BO_4 tetrahedron, resulting in a highly cross-linked network. Therefore, the Bi_2O_3 will affect the borate network as follows. Increasing Bi_2O_3 content yields a series of distorted dipentaborate groups connected by the bismuth cations, and the excess oxygen anions will balance the charge. The intensities of the bands at 490–520 cm^{-1} of distorted $[BiO_6]$ octahedral units increase, and the bands of $[BO_4]$ and $[BO_3]$ units are shifted to lower wavenumber. This behavior can be explained by taking into account the observed shift to higher wavenumber in the band from 701 to 715 cm^{-1} (belonging to the bending vibration of B–O–B in $[BO_3]$ units). According to Cheng *et al* [15], this shift may be introduced by the electrostatic field of the strongly polarizing Bi^{2+} ions. The raising of Bi_2O_3 content results in an increase in the electron cloud density around the oxygen in the $[BO_3]$ unit, thus it leads to an increase in the roll-torque of the B–O–B band and consequently it contributes to the bending vibration of the B–O–B band shifting to a higher wavenumber. Thus, a new bridging bond of Bi–O–B will be formed due to the inducement of the aforementioned electrostatic field. The stretching force constant of this bond tends to decrease, since the stretching force constant of Bi–O bonding is lower than that of B–O bonding [15, 35, 39–41]. Accordingly, the bond length of Bi–O bonding increases (equation (2)), increasing the molar volume [5]. On the other hand, increasing the Bi_2O_3 content in the range $30 \leqslant x \leqslant 45$ mol% results in some constancy in the stretching force constant of the $[BO_3]$ structural unit (figure 3). This behavior is attributed to less destruction of distorted dipentaborate groups, and the thermal stability against crystallization in these glasses. A further increase in the Bi_2O_3 content beyond $x = 45$ mol% causes a weakening of the borate network, as discussed before [5], so the stretching force constant of $[BO_3]$ will decrease.

4.2. Thermal analysis and thermal stability of glass

Before discussing the thermal parameters of the glasses that were studied, it is worth mentioning that, at 30 Bi_2O_3 content, there is a poor trend in crystallization, so the thermal treatment was quoted for the $35 \leqslant x \leqslant 60$ glasses. Figure 4(a)

Table 2. The values of thermal parameters of glass transition temperature T_g, onset temperature of crystallization T_{in}, crystallization temperature T_p and melting temperature T_m of $x Bi_2O_3 \cdot (100 - x) B_2O_3$ ($35 \leqslant x \leqslant 60$) alloys with different heating rates β. The characteristic parameters K_{gl}, H_r and S are according to the text.

Alloy	β	T_g (K)	T_{in} (K)	T_p (K)	T_m (K)	K_{gl}	H_r	H'	S (K)
$x = 35$									
	5	711	849	868	987	1	1.16	0.194	3.688
	10	720	860	879	997	1.022	1.186	0.194	3.694
	20	731	872	890	1009	1.029	1.185	0.193	3.472
	30	737	877	897	1019	0.986	1.148	0.19	3.799
	40	743	882	904	1028	0.952	1.121	0.187	4.116
$x = 40$									
	5	674	798	816	937	0.892	1.025	0.184	3.312
	10	684	809	826	947	0.906	1.033	0.183	3.107
	20	696	821	836	959	0.906	1.016	0.18	2.694
	30	702	826	842	969	0.867	0.976	0.177	2.826
	40	708	831	847	978	0.837	0.939	0.174	2.78
$x = 45$									
	5	649	756	774	892	0.787	0.907	0.165	2.968
	10	660	767	784	902	0.793	0.907	0.162	2.756
	20	673	779	794	914	0.785	0.883	0.158	2.363
	30	678	784	800	924	0.757	0.855	0.156	2.501
	40	685	789	805	933	0.722	0.813	0.152	2.429
$x = 50$									
	5	645	733	751	863	0.677	0.786	0.136	2.456
	10	657	744	761	873	0.674	0.777	0.132	2.251
	20	670	756	771	885	0.667	0.754	0.128	1.925
	30	675	761	777	895	0.642	0.729	0.127	2.039
	40	682	766	782	904	0.609	0.689	0.123	1.971
$x = 55$									
	5	640	709	728	848	0.496	0.575	0.108	2.048
	10	653	720	738.9	858	0.486	0.563	0.103	1.939
	20	665	732	749.5	870	0.486	0.556	0.101	1.763
	30	672	737	756.1	880	0.455	0.525	0.097	1.847
	40	678	742	761.7	889	0.435	0.503	0.094	1.860
$x = 60$									
	5	633	691	703	837	0.397	0.433	0.092	1.1
	10	646	702	713	847	0.386	0.418	0.087	0.954
	20	660	714	723	859	0.372	0.397	0.082	0.736
	30	666	719	729	869	0.353	0.379	0.080	0.796
	40	673	724	734	878	0.331	0.354	0.076	0.758

shows the DTA thermograms for amorphous $35Bi_2O_3$–$65B_2O_3$ glass recorded at different heating rates. The characteristic feature of this thermogram is the homogeneity of the glass being considered, which is confirmed by the appearance of a small single endothermic peak. This peak is attributed to the glass transition temperature, which represents the strength or rigidity of the glass structure. Also, there is an exothermic peak originating from the amorphous–crystalline transformation. The exothermic peak has two characteristic points: the first point is the onset temperature of crystallization (T_{in}) and the second is the peak temperature of crystallization (T_p). This figure also shows the characteristic melting temperatures, T_m.

The inset figure 4(b) shows the DTA thermograms for amorphous $35Bi_2O_3$–$65B_2O_3$ glass recorded at a rate of 5 K min^{-1}. This figure shows the glass transition temperature, T_g, the onset temperature of crystallization, T_{in}, the crystallization temperature, T_p, and the melting temperature, T_m. The characteristic temperatures T_g, T_{in}, T_p, and T_m for $x Bi_2O_3$–$(100 - x) B_2O_3$ ($35 \leqslant x \leqslant 60$) glasses are given in table 2. The glass forming ability of the glasses that were studied can be estimated by using these characteristic temperatures. The existing stability criterion parameters based on these characteristic temperatures, H_r, H' and S, for different composition are listed in table 2. It is found that the values of these criteria decrease with increasing Bi_2O_3 content. Bearing in mind that the values of these parameters increase with increasing stability, it is possible to suggest that the higher the Bi_2O_3 content of the alloy, the lower is its glass thermal stability [40, 41]. The deduced values of k_{gl} for the different compositions are listed in table 2. The decreasing values of T_g with increasing Bi_2O_3 content are assigned for the following reasons. The increase in the inter-ionic bond distance is attributed to the larger ionic size of Bi^{3+} (0.108 nm) than that of B^{3+} (0.02 nm) [42]. The bond strength plays a competitive role in decreasing T_g. The bond strengths of B–O and Bi–O are 192.7 kcal mol^{-1} and 80.3 kcal mol^{-1}, respectively [41], so the decrease in T_g is attributed to the replacement of a B–O linkage by the weaker Bi–O linkage. Similarly, the observed decrease in T_g for the glasses that were studied may be due to the increasing number of non-bridging oxygen atoms.

The determination of the so-called activation energy of enthalpy relaxation of the glass transition, or activation energy of glass transition E_g of the investigated glass, can be

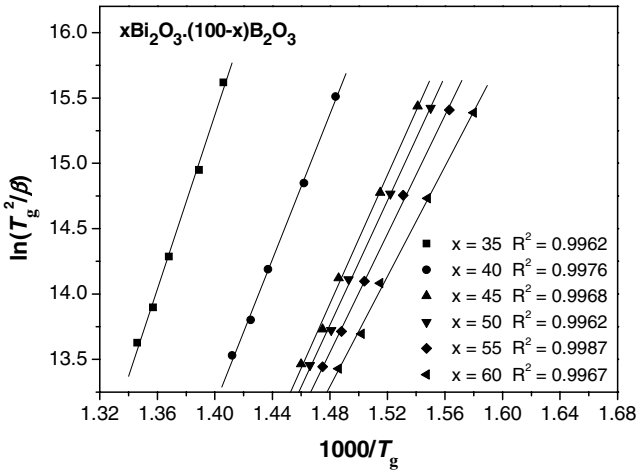

Figure 5. Plot of $\ln T_g^2/\beta$ versus $1000/T_g$ of the analyzed materials. The values of correlation coefficients (R^2) are also presented.

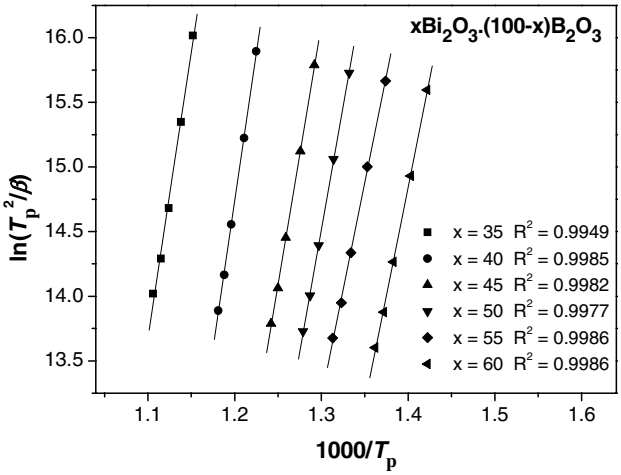

Figure 7. Experimental plot of $\ln T_p^2/\beta$ versus $1000/T_p$ and straight regression lines for the different glassy alloys (β in K s^{-1}). The values of correlation coefficients (R^2) are also presented.

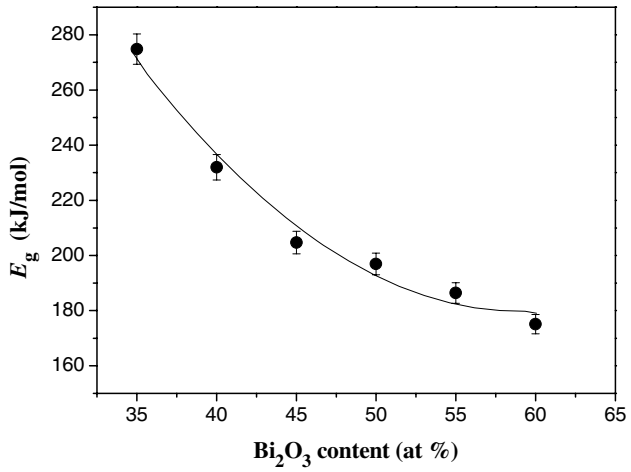

Figure 6. Activation energy of transition E_g as a function of Bi content in $x\mathrm{Bi_2O_3}$–$(100-x)\mathrm{B_2O_3}$ ($35 \leqslant x \leqslant 60$) glassy system.

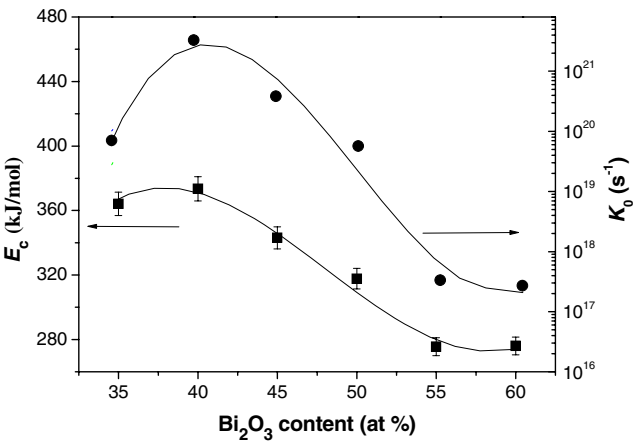

Figure 8. The activation energy of crystallization, E_c, and frequency factor, K_0, of the analyzed alloys obtained from the straight regression lines fitted to values of $\ln T_p^2/\beta$ versus $1000/T_p$. The error related to K_0 is smaller than the size of the symbol.

performed using the Kissinger formula, which was originally derived for the crystallization process and is suggested to be valid for glass transition [43]. This formula has the following form,

$$\ln(T_g^2/\beta) = E_g/RT_g + \text{const} \tag{9}$$

where R is the universal gas constant. There is a straight line between $\ln(T_g^2/\beta)$ and $1/T_g$ for different compositions whose slopes yield a values of E_g (figure 5), where the subscript g denotes the magnitude values corresponding to the glass transition temperature. Figure 6 shows the decreasing trend in E_g with the increase in Bi_2O_3 content.

For evaluating the activation energy for crystallization (E_c) using the variation in T_p with β, Vázquez *et al* [33] developed the proposed method by Kissenger [43] for non-isothermal analysis of devitrification as follows:

$$\ln[T_p^2/\beta] = E_c/RT_p + \ln(E_c/RK_0). \tag{10}$$

Figure 7 represents the evolution of $\ln(T_p^2/\beta)$ versus $1/T_p$ for different compositions. The plots were found to be straight lines. The activation energy, E_c, and the frequency factor, K_0, are then evaluated using the least-squares fitting method. Figure 8 shows values for both E_c and K_0 as a function of Bi_2O_3 content. The trend in activation energy for crystallization (E_c) can be interpreted in terms of the glass structure as follows. Increasing the Bi_2O_3 content in the range $35 \leqslant x \leqslant 45$ results in some constancy in E_c, which decreases as the Bi_2O_3 content increases beyond $x = 45$. This behavior is in accordance with the stretching force constant of $[BO_3]$ behavior.

After determining the values of E_c and K_0, the kinetic parameters $K(T)$ and $K_r(T)$ of the glasses that were studied were calculated using equations (3) and (5), respectively. These calculations were carried out in order to compare the stability sequence of the glasses that were studied from the quoted parameters with the corresponding sequence deduced from the stability criteria based on characteristic temperatures. The values of $K(T_g)$ and $K_r(T_p)$ for the temperatures T_g and T_p

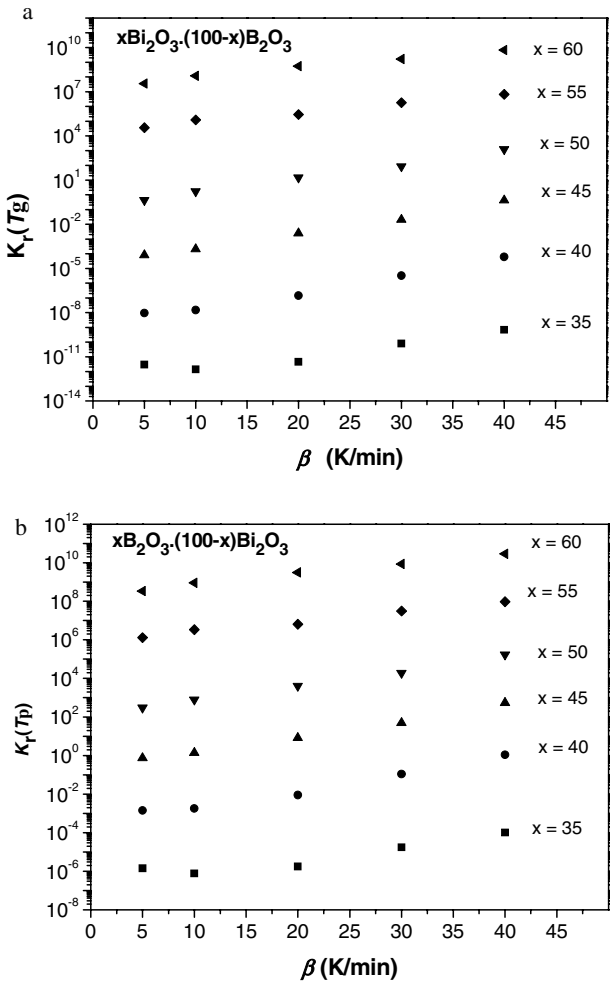

Figure 9. (a) Plots of $K_r(T_g)$ versus β for different glass compositions and (b) plots of $K_r(T_p)$ versus β for different glass compositions to verify the stable order.

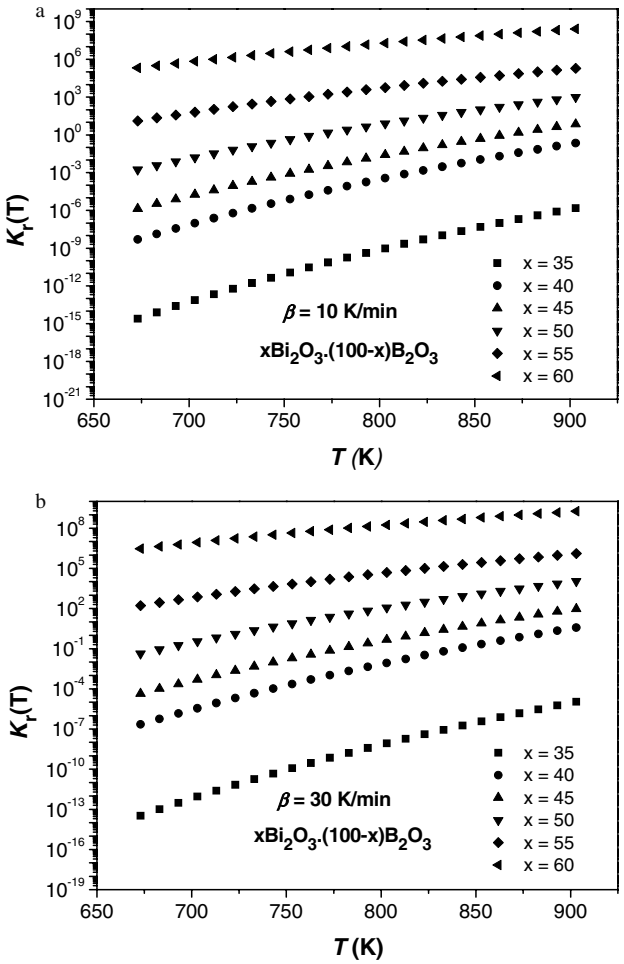

Figure 10. Plots of $K_r(T)$ versus T for the different glassy alloys to confirm the stable order: (a) $\beta = 10$ K min^{-1}, and (b) $\beta = 10$ K min^{-1}.

were calculated and plotted with the heating rates β as shown in figures 9(a) and (b). According to the literature [38–40], the smaller the values of $K(T_g)$ and $K(T_p)$ criteria, the better should be the glass forming ability of the material. So, the data for both $K(T_g)$ and $K(T_p)$ in the former figures indicate that the thermal stability decreases with increasing Bi_2O_3 content.

Figures 10(a) and (b) represent the plots of $K_r(T)$ versus T for the different glass compositions to confirm the stable order at $\beta = 10$ and 30 K min^{-1}. It is found that $K_r(T)$ increases with increasing temperature. These two figures display that $K_r(T)$ increases with increasing Bi_2O_3 content, i.e. the thermal stability decreases with increasing Bi_2O_3 content.

4.3. Crystallization rate and kinetic exponent

The theoretical basis for interpreting DTA results is provided by the formal theory of transformation kinetics, as developed by Johnson *et al* [44] and Avrami [45, 46]. The fraction, χ, crystallized at a given temperature, T, is given by $\chi = A_T/A$, where A is the total area of the exothermic between the temperature T_i (crystallization is just beginning) and the temperature T_f (the crystallization is completed), and A_T is the area between T_i and T, as shown in figure 11. The graphical representation of the crystallized volume fraction of $35Bi_2O_3{\cdot}65B_2O_3$ at different heating rates shows the typical sigmoid curve as a function of temperature (figure 12) in crystallization reactions [47, 48].

The ratio between the ordinates of the DTA curve and the total area of the peak gives the corresponding crystallization rates, which makes it possible to build the curves of the exothermal peaks represented in figure 13 for the $35Bi_2O_3{\cdot}65B_2O_3$ sample. It may be observed that the $(dx/dt)_p$ values increase as well as the heating rate, which is a property that has been widely discussed in the literature [49]. From the experimental values of $(dx/dt)_p$, one can calculate the kinetic exponent n by using the following equation:

$$(d\chi/dt)_p = n(0.37\beta E_c)/(RT_p^2). \qquad (11)$$

The n values for the glasses that were studied are calculated and listed in table 3. Finally, the experimental data, T_p, and $(dx/dt)_p$, listed in tables 2 and 3, respectively, and the above-mentioned value of the activation energies of crystallization process for the crystallization peaks, makes it possible to determine, through relationship (11), the kinetic

Table 3. Maximum crystallization rate ($d\chi/dt$), kinetic exponent n and average kinetic exponent $\langle n\rangle$ for $x Bi_2O_3{\cdot}(100-x)B_2O_3$ ($35 \leqslant x \leqslant 60$) alloys with different heating rates β.

	x											
	35		40		45		50		55		60	
β (K min^{-1})	$(d\chi/dt)$ (10^{-3} s^{-1})	n	$(d\chi/dt)$ (10^{-3} s^{-1})	n	$(d\chi/dt)$ (10^{-3} s^{-1})	n	$(d\chi/dt)$ (10^{-3} s^{-1})	n	$(d\chi/dt)$ (10^{-3} s^{-1})	n	$(d\chi/dt)$ (10^{-3} s^{-1})	n
5	5.617	3.158	4.428	2.121	4.346	2.081	4.1	1.965	3.555	1.845	4.15	2.0
10	12	3.369	9.234	2.266	8.533	2.096	8.05	1.981	7.245	1.932	8.45	2.096
20	22	3.305	18	2.226	17	2.19	16	2.071	15	2.021	17	2.195
30	31	3.078	24	2.075	24	2.043	23	1.932	20	1.887	24	2.05
40	37	2.809	29	1.895	29	1.867	27	1.767	26	1.821	30	1.98
$\langle n\rangle$		3.144± 0.070		2.117± 0.069		2.055± 0.057		1.943± 0.057		1.901± 0.043		2.046± 0.042

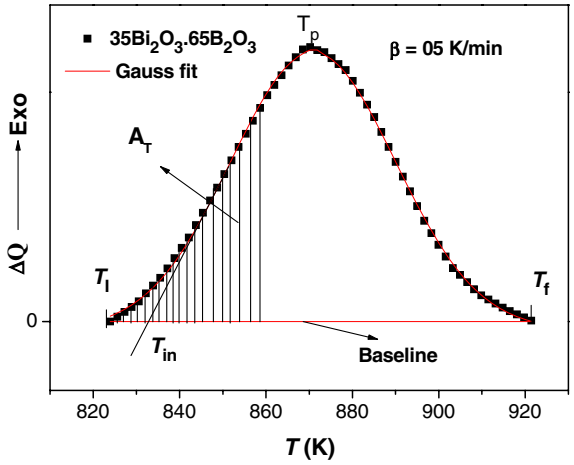

Figure 11. DTA traces for $35Bi_2O_3{\cdot}65B_2O_3$ glass at a heating rate of 5 K min^{-1}; the lined area A_T shows between T_i and T_f of the peak. T_i, T_f and T are according to the text.

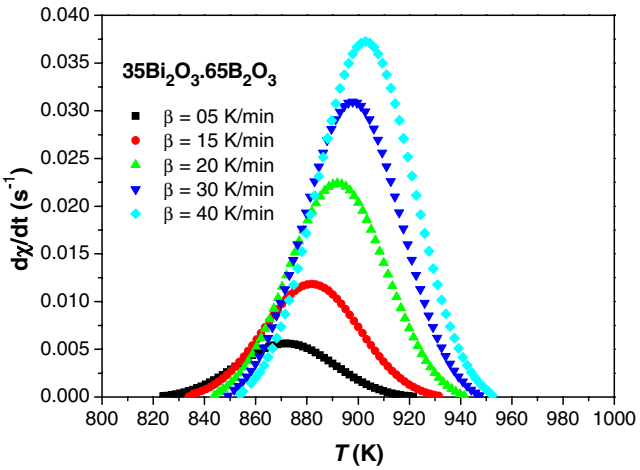

Figure 13. Crystallization rate versus temperature of the exothermal peaks for $35Bi_2O_3{\cdot}65B_2O_3$ glass at different heating rates.

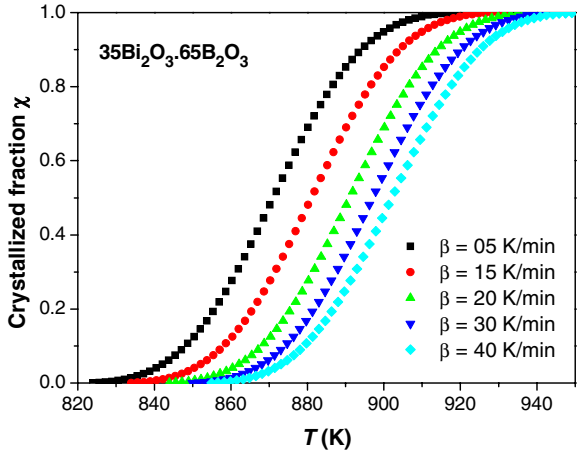

Figure 12. Crystallized fraction as a function of temperature for $35Bi_2O_3{\cdot}65B_2O_3$ glass composition at different heating rate.

exponent, n, for each one of the experimental heating rates corresponding to the peaks for each glass sample, whose values are also given in table 3. Taking into account the experimental error, the values of $\langle n\rangle$ are close to 3 for $35Bi_2O_3{\cdot}65B_2O_3$ glass and close to 2 for the other compositions. The kinetic exponent was deduced on the basis of the mechanism of crystallization [50]. According to Mahadevan *et al* [51], n may be 4, 3, 2, or 1, which are related to the different glass–crystal transformation mechanisms: $n = 4$, volume nucleation, three-dimensional growth; $n = 3$, volume nucleation, two-dimensional growth; $n = 2$, volume nucleation, one-dimensional growth; $n = 1$, surface nucleation, one-dimensional growth from surface to the inside. Therefore, bearing in mind the above obtained mean value, $\langle n\rangle = 2$ for the crystallization peaks means volume nucleation, one-dimensional growth.

5. Conclusions

Increasing the Bi_2O_3 content at the expense of B_2O_3 in the glass system that was studied reveals some remarkable features:

(1) According to the infrared analysis, there is some constancy in the vibrations of $[BO_3]$ and hence the behavior of its corresponding stretching force constant in the range $30 \leqslant x \leqslant 45$ mol%, indicating an expected thermal stability of the glass, while beyond $x = 45$ the

behavior differs because of the weakening of the structure and the increasing tendency for crystallization.

(2) The various thermal stability criteria K_{gl}, H_r, H' and $S(K)$ (based on characteristic temperatures T_g, T_{in}, T_p and T_m) decrease with increasing Bi_2O_3 content, reflecting the decrease in thermal stability.

(3) The deduced values of k_{gl} for the different compositions reveal that the glass forming ability decreases with increasing Bi_2O_3 content. This effect implies a greater crystallization tendency in glasses containing larger concentrations of Bi_2O_3.

The values of the kinetic parameters $K(T_g)$, $K(T_p)$ and $K_r(T)$ increase with increasing Bi_2O_3 content; this means and confirms that the thermal stability decreases with increasing Bi_2O_3 content, at the expense of B_2O_3.

Acknowledgment

The authors thank the Faculty of Science at Al Azhar University (Assiut-Egypt) for financial support.

References

[1] Shelby J E 1997 *Introduction to Glass Science and Technology* (UK: The Royal Society of Chemistry)
[2] Varshneya A 1994 *Fundamentals of Inorganic Glasses* (New York: Academic)
[3] Yano T, Kunimine N, Shibata S and Yamane M 2003 *J. Non-Cryst. Solids* **321** 137
[4] Stone C, Wright A, Sinclair R, Feller S, Affatigato M, Hogan D, Nelson N, Vira C, Dimitriev Y, Gattef E and Ehrt D 2000 *Phys. Chem. Glasses* **41** 409
[5] Stehle C, Vira C, Hogan D, Feller S and Affatigato M 1998 *Phys. Chem. Glasses* **39** 83
[6] Wells A 1975 *Structural Inorganic Chemistry* 4th edn (Oxford: Clarendon)
[7] Vogel W 1985 *Chemistry of Glass* (Westerville, OH: American Ceramic Society)
[8] Baia L, Stefan R, Popp J, Simon S and Kiefer W 2003 *J. Non-Cryst. Solids* **324** 109
[9] Simon S and Todea M 2006 *J. Non-Cryst. Solids* **352** 2947
[10] Gowda V, Reddy C, Radha K, Anavekar R, Etourneau J and Rao K 2007 *J. Non-Cryst. Solids* **353** 1150
[11] Venkataraman B and Varma K 2006 *Opt. Mater.* **28** 1423
[12] Borsa F, Torgeson D, Martin S and Patel H 1992 *Phys. Rev.* B **46** 795
[13] Dimitriev Y, Mihailova V and Gattef E 1986 *Phys. Chem. Glasses* **34** 114
[14] Mianxue W and Peinan Z 1986 *J. Non-Cryst. Solids* **84** 344
[15] Cheng Y, Xiao H, Guo W and Guo W 2006 *Thermochim. Acta* **444** 173
[16] Zheng H and Mackenzie J 1988 *Phys. Rev.* B **38** 7166
[17] Zheng H, Xu R and Mackenzie J 1989 *J. Mater. Res.* **4** 911
[18] Hall D, Newhouse M, Borrelli N, Dumbaugh W and Weidman D 1989 *Appl. Phys. Lett.* **54** 1293
[19] Onishi M, Kyoto M and Watanabe M 1991 *Japan. J. Appl. Phys.* **30** L988
[20] Dumbaugh W 1978 *Phys. Chem. Glasses* **19** 121
[21] Simon S and Todea M 2006 *J. Non-Cryst. Solids* **352** 2947
[22] Fu J and Yatsuda H 1995 *Phys. Chem. Glasses* **36** 211
[23] Fu J 1996 *Phys. Chem. Glasses* **37** 84
[24] Pan A and Ghosh A 2002 *J. Mater. Res.* **17** 1941
[25] Bridge B and Higazy A A 1986 *Phys. Chem. Glasses* **27** 1
[26] Dietzel A 1968 *Glasstech. Ber.* **22** 41
[27] Sakka S and Mackenzie J D 1971 *J. Non-Cryst. Solids* **6** 145
[28] Hruby A 1972 *Czech. J. Phys.* B **22** 1187
[29] Saad M and Poulain M 1987 *Mater. Sci. Forum* **19/20** 11
[30] Yinnon H and Uhlmann D R 1983 *J. Non-Cryst. Solids* **54** 253
[31] Surinach S, Baro M D, Clavaguera-Mora M T and Clavaguera N 1984 *J. Mater. Sci.* **19** 3005
[32] Hu L and Jiang Z 1990 *J. Chin. Ceram. Soc.* **18** 315
[33] Vàzquez J, López-Alemany P L, Villares P and Jiménez-Garay R 2003 *J. Alloys Compounds* **354** 153
[34] Kamitsos E, Karakassides M and Chryssikos G 1987 *J. Phys. Chem.* **91** 1073
[35] Kamitsos E, Patsis A, Karakassides M and Chryssikos G 1990 *J. Non-Cryst. Solids* **126** 52
[36] Chryssikos G, Liu L, Varsamis C and Kamitsos E 1998 *J. Non-Cryst. Solids* **235** 761
[37] Baia L, Stefan R, Kiefer W and Simon S 2005 *J. Raman Spectrosc.* **36** 262
[38] Chowdari B and Rong Z 1996 *Solid State Ion.* **90** 151
[39] Moustafa Y, Doweidar H and El-Damrawi G 1994 *Phys. Chem. Glasses* **35** 104
[40] Baia L, Stefan R, Kiefer W, Popp J and Simon S 2002 *J. Non-Cryst. Solids* **303** 379
[41] Lide D 2004 *CRC Handbook of Chemistry and Physics* 84th edn (Boca Raton, FL: CRC Press)
[42] Moody B 1991 *Comparative Inorganic Chemistry* 3rd edn (UK: Butterworth-Heinemann)
[43] Kissinger H E 1957 *Anal. Chem.* **29** 1702
[44] Johnson W and Mehl R 1939 *Trans. Am. Inst. Min. Met. Eng.* **135** 416
[45] Avrami M 1940 *J. Chem. Phys.* **8** 212
[46] Avrami M 1941 *J. Chem. Phys.* **9** 177
[47] Ligeno R A, Vazquex J, Casns-Ruix M and Jirnenez-Caray R 1992 *Thermochim. Acta* **197** 319
[48] Wagner C, Villanes P, Vazquex J and Jirnenex-Caray R R 1993 *Mater. Lett.* **19** 370
[49] Gao Yi Qun, Wang W, Zheng F Q and Liu X 1986 *J. Non-Cryst. Solids* **81** 135
[50] Matusita K and Saka S 1980 *J. Non-Cryst. Solids* **38/39** 741
[51] Mahadevan S, Giridhar A and Sing A K 1986 *J. Non-Cryst. Solids* **88** 11